Plasmonics (2023) 18:2475–2482
https://doi.org/10.1007/s11468-023-01960-4

RESEARCH

Quantitative Analysis of High Performance Plasmonic Metamolecules for Targeted Deep Tissues Applications

Sajid Farooq[1,2] · Diego Rativa[2,3,4] · Renato E. de Araujo[5]

Received: 18 June 2023 / Accepted: 18 July 2023 / Published online: 28 July 2023

Abstract

Rationally designed gold nanoparticles (Au NPs) show a great potential for biomedical applications. Specifically, for optically induced heating of deep tissues facilitated by plasmonic-assisted lasers, nanostructures with high optical absorption coefficient in biological window are required. Plasmonic metamolecules, such as gold nanodimers (NDs), exhibit a robust localized field enhancement with strong infrared optical absorption. However, an exclusive investigation of the optical/thermal features of high-performance Au NDs for optical infrared heating remains a challenge. Here, we focus on Au NDs for optothermal characteristics in deep tissues heating procedures. Our analysis encompasses parameters such as absorption cross-sections, field enhancement, and temperature rise with a systematic methodology selecting optimal NDs. Our findings reveal a non-uniform spatial distribution of temperature at the nano-scale and show that short-pulsed laser excitation enhances the temperature near the dimer's junction. Remarkably, when compared to monomeric gold nanorods under the same excitation resonance mode, optically generated heating of Au NDs leads a threefold higher temperature increase. These results evidence valuable insights for using Au NDs as efficient plasmonic nanoheaters in photothermal-assisted applications.

Keywords Metallic metamolecules · Optical therapy · Nanoheaters

Introduction

Due to exceptional optical absorption properties, metallic nanoparticles (NPs) have gained significant attention as advanced materials in diverse fields such as bio-medicine, nano-catalysis, chemical separation, and solar-heat transducers [1–6]. By leveraging the electromagnetic coupling with metallic sub-wavelength NPs, they can induce localized surface plasmon resonance (LSPR). This phenomenon allows precise control of light absorption and scattering across the visible to near-infrared (NIR) spectrum, accompanied by a robust near-field enhancement [7–10]. The shape, material compositions, size, and orientation of metallic NPs directly impact their LSPR characteristics, providing opportunities for tailored applications and improved performance in various scientific and technological domains [11]. Optical light absorption by noble metal NPs can also be nonradiative converted into heat. Subsequently, thermal energy will be released to the surrounding medium through conductive contribution, causing the NP to act as a nanoheater. The conversion of light to thermal energy by metallic NPs has been extensively used for photothermal applications. Moreover, plasmonic nanoparticles can be employed as an efficient heat generator for uniform and controlled thermal release to the surrounding at a particular excitation wavelength [12]. In particular, for deep in situ optical heating of NPs, an infrared LSPR phenomenon within biological window ($\lambda = 650 - 1350$ nm) is required, which can be achieved by tuning the morphology of the particles as well as their dimensions during the synthesis procedures [13, 14].

A plethora of literature reveals that metallic NPs with complex geometries have been synthesized in colloids with

✉ Sajid Farooq
sajiddahar@gmail.com; sajid.f@ipen.br

1 Center for Lasers and Applications, Energy and Nuclear Research Institute (IPEN), Av. Prof. Lineu Prestes 2242, São Paulo 05508-000, Brazil

2 Institute of Technological Innovation, University of Pernambuco, Recife, PE, Brazil

3 Polytechnic School of Pernambuco, University of Pernambuco, Recife, PE, Brazil

4 Applied Physics Program, Federal Rural University of Pernambuco, Recife, Brazil

5 Laboratory of Biomedical Optics and Imaging, Federal University of Pernambuco, Recife, Brazil

fine control for several photothermal applications. Nanoparticles with complex shapes such as bipyramids, rattle, plates, rods, and stars are also manipulated for NIR photo-assisted therapy [15–17]. However, most structures lack high photothermal conversion efficiency due to low absorption or high scattering at the NIR regime. Recently, Schumacher et al. suggested that metallic particles separated by a nanometer gap, also named metamolecules or plasmonic dimers, is an alternative design for plasmonic-related application [18]. Nanodimers' geometry structures (NDs) exhibit highly robust localized field enhancement in the nanogap regions, commonly termed as "hot spots" [19, 20]. These hot spots in the nanogap domains increase while decreasing the interparticle distance until the quantum-tunneling limit [21]. Consequently, the LSPR phenomenon observed in Au NDs with active hot spots exhibits a highly desirable and accessible characteristic for photothermal applications.

Currently, significant efforts have been devoted to the improvement of nanofabrication techniques capable of synthesizing plasmonic NDs on substrates or in colloidal solutions. Hao et al. successfully fabricated plasmonic dimeric arrays with ultra-small nanogaps using ultra-thin anodic-aluminum oxide membranes [22]. Similarly, Zheng et al. explored nanofabrication methods to create discrete symmetric and non-symmetric gold dimeric arrays supported by substrates [23]. To generate arrays of periodic metallic NPs, researchers have also explored top-down lithography techniques, including electron-beam lithography and angle-resolved nanosphere lithographic techniques [24, 25]. However, these lithographic methods are often considered expensive and are limited in their scalability for large-scale applications. In an alternative approach, Fontana et al. demonstrated the synthesis of plasmonic NDs where the NPs are coupled end-to-end using a dielectric junction [26]. This novel method offers a new avenue for the controlled assembly of plasmonic dimers in colloid. These advancements in nanofabrication methods provide valuable tools for manipulating plasmonic NDs and pave the way for further exploration and utilization in various scientific and technological applications. The reported dimer has approximately 1 nm long gap, which is approximately the length of the molecule use to link together the nanorods. In another study, Yoon et al. proposed a promising method for fabricating asymmetric plasmonic NDs in colloidal solutions. This approach offers the potential to induce unique functionality and obtain desired optical and magnetic properties [27]. In addition, Chen et al. conducted ensemble-averaged measurements of hotspots by precisely controlling the synthesis of uniform dimers and trimers of metamolecules [28]. However, it is vital to understand that these previous studies primarily focused on the optical properties of metallic metamolecules, and further attention needs to be given to the thermo-plasmonic behavior of colloidal metamolecules for thermal-assisted applications. Despite their contributions, the existing literature mostly presents qualitative behavior or empirical data, emphasizing the need for a more systematic analysis [14, 29, 30].

Here, we evaluate the thermoplasmonic features of Au dimeric shaped metamolecules (nanorods joined end to end by dielectric junction). A computational modeling framework based on finite element methods is applied on the analysis of the optical absorption, localized field enhancement, and temperature increase of the dimeric metamolecules as function of their aspect ratios. The photothermal performance of laser-heated metamolecules is quantified by the Joule number factor, and the heating dynamic of colloidal metamolecules is also apprised.

Materials and Methods

Numerical Simulations

To evaluate the optothermal properties of NDs, a comprehensive 3D full-wave field analysis was conducted using the finite element method (FEM) with the radio frequency (RF) module in COMSOL Multiphysics software. Figure 1a presents the structure of an individual nanorod (NR), which is based on hemispherically capped cylinders with a length (L) and a diameter (D). In the simulation, the diameter of the nanorod (D) was kept constant at 10 nm, while the length (L) was tuned to investigate its influence. The metallic ND configuration was created by assembling two Au NRs with a thin dielectric cylindrical junction. The aspect ratio (AR) of both the gold monomer and the dimer was defined as the ratio of the diameter to the nanorod's length, as depicted in Fig. 1a. The aspect ratio of the monomer nanorod (ARm) was L/D, while the dimeric nanostructure's aspect ratio (ARd) was defined as Leff/D, where the effective length (Leff) was calculated as 2 L+g. Here, g represents the thickness and length of the dielectric cylindrical junction, which were both set to 1 nm, with a refractive index (n) of 1.46. In the computational modeling domain, as shown in Fig. 1b, the gold nanoparticle was set at the origin (0, 0, 0) of a spherical coordinate system, encompassed by a dielectric medium, specifically water with a refractive index of 1.33. To mitigate back-scattering effects, a perfectly matched layer (PML) with a thickness of 250 nm was implemented around the domain. An incident linearly polarized plane wave (E = 1 Vm^{-1}) propagated in the z-direction towards the nanoparticle. The incident field was p-polarized at normal incidence, with the electric field (E-field) aligned along the x-axis (the longest dimension axis of the nanorod) and the magnetic field (H-field) aligned along the y-axis. The time-harmonic E-field within the domain was described by a suitable mathematical representation [13].

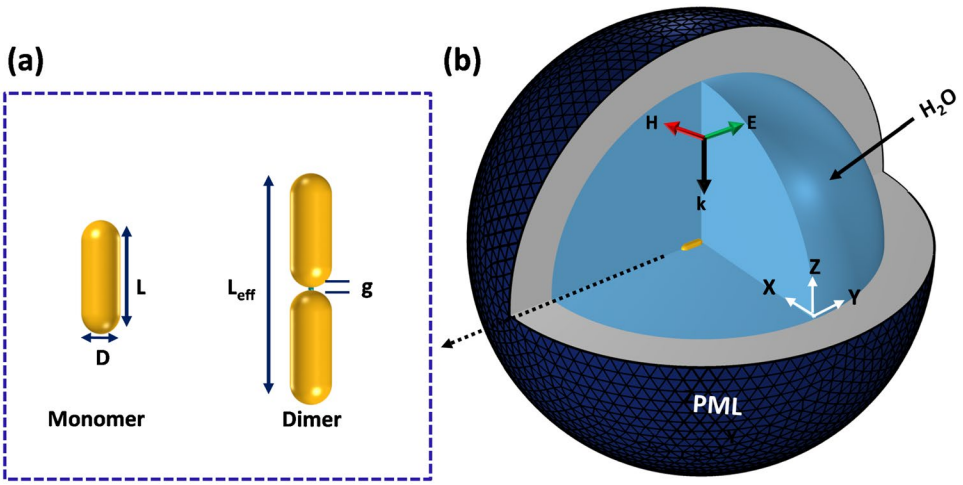

Fig. 1 The metallic NPs and numerical modeling geometry consisted of monomer and dimer rods (**a**), while a 3D spherical computational domain with a perfectly matched layer (PML) was employed to represent the propagation direction and polarization of the incident field (**b**). The gold nanorod (Au NR) was positioned at the center of the computational domain and surrounded by the dielectric medium, water (H_2O)

$$\nabla \times \left(\frac{1}{\mu_r}\nabla \times E\right) - {k_0}^2\left(\epsilon_r - j\frac{\sigma}{\omega\epsilon_0}\right)E = 0, \tag{1}$$

where, σ denotes the conductivity, ϵ_r represents the dielectric function, and μ_r indicates the permeability of the surrounding medium. Furthermore, k_0 denotes the wavenumber in free space.

The experimental data by Johnson and Christy [31] acquire the real and imaginary values of permittivity for Au. However, when dealing with small Au/Ag NPs, the impact of electron-interface scattering becomes significant, leading the consideration of size-dependent corrections for the permittivity, represented as ϵ_{NP} [13]:

$$\epsilon_{NP}(\omega, L_{eff}) = \epsilon_{bulk}(\omega) + \frac{{\omega_p}^2}{\omega^2 + i\omega\gamma_0} - \frac{{\omega_p}^2}{\omega^2 + i\omega(\gamma_0 + AV_f/L_{eff})}, \tag{2}$$

In order to study fundamental properties of the materials, numerous key parameters play a crucial role such as plasma frequency (ω_p) and Fermi velocity (V_f). Additionally, γ_0 denotes a phenomenological scattering parameter that characterizes the interaction of electrons with various factors such as phonons, lattice defects, electrons, or impurities within the bulk material. For Au, γ_0 is reported as $1.07 \times 10^{14} s^{-1}$, while V_f is determined to be $1.40 \times 10^6 ms^{-1}$ [32]. Furthermore, a dimensionless parameter denoted as A is introduced, which typically has a value close to unity. Additionally, for particles with convex shapes like spheres or rods, the effective electron path length, L_{eff}, can be expressed as $L_{eff} = 4V/S$, where V represents the volume of the nanoparticle and S corresponds to its surface area [13]. To achieve the optical absorption cross-section values of NPs, the dielectric functions were explored in this study [32].

Optical Cross-section Calculations

As mentioned earlier in Eq. (1), the solution of Maxwell's equations was applied to derive the absorption (σ_{abs}), scattering (σ_{sca}), and extinction (σ_{ext}) cross-sections. The optical cross-sections can be expressed, given as [33].

$$\sigma_{sca} = \frac{1}{I_0}\int\int(\mathbf{n}.S_{sca})dS, \tag{3}$$

$$\sigma_{abs} = \frac{1}{I_0}\int\int\int QdV, \tag{4}$$

$$\sigma_{ext} = \sigma_{abs} + \sigma_{sca}, \tag{5}$$

where the vector **n** presents normal from the center of NP, Q is heat-loss density, S_{sca} is the scattered-intensity vector over domain surface area (S), V is the volume of the particle, and $I_0(W/m^2)$ is the incident laser irradiance [33]. To validate our results obtained through computational FEM modeling, the Gans theory was used as a benchmark [19].

Thermal Analysis

In order to explore the thermal behavior of NPs and their effects in surrounding, we used the time-dependent (transient heat transfer) equation, denoted as [34]:

$$C_p\rho\frac{\partial T}{\partial t} + \nabla\cdot(-k\nabla T) = Q, \tag{6}$$

where the heat capacity of Au (C_p) is 129 (J/kg/K), the density (ρ) is 19.32 ($\times 10^3 kg/m^3$), and the thermal conductivity (k) is 0.60 (W/m/K). The heating power per unit volume, termed as Q, is given by the product of the absorption

cross-section (σ_{abs}) and the incident power density (I_0). Although, the temperature (T) of the NPs is both time and space-dependent, representing its thermal response. The thermal analysis were performed using the heat transfer in solids module in COMSOL. This module focuses on modeling the heating of the material, providing temperature information as the output. To meet the requirements of the model, a spherical perfectly matched layer (PML) domain and appropriate boundary conditions were selected. The nanoparticles were subjected to 20 ns laser irradiation at 1064 nm and with optical power of $1x10^9$ W.

Results and Discussion

Optical Properties of Au Nanostructure

Figure 2 depicts the optical cross-sections of absorption and scattering for monomers and dimeric structures for different aspect ratios, considering a diluted aqueous solution, i.e., ignoring inter-particle interaction. It can be seen that enlarging ARs of monomers from 2.1 to 12.1 consequently increases the LSPR peak wavelength from NIR to the mid-IR regime (600 to 1700 nm). Moreover, the optical absorption of Au NRs also tunes and depends on geometric parameters. Similar behavior can be expounded for Au NDs, where the plasmonic peak shifts into the biological window, as identified in Fig. 2b. The ability to tune NIR radiation is beneficial for laser-based theranostic applications, facilitating precise targeting and manipulation of biological systems and making it a sought-after attribute in the field of theranostics.

Furthermore, it is observed that both monomers and dimers exhibit high optical absorption values ($3 \times 10^{-15}\ m^2$) when their aspect ratio exceeds 5. However, NDs demonstrate higher absorption cross-section (σ_{abs}) values at the peak resonance wavelengths compared to monomers. Additionally, a significant distinction can be seen in the scattering cross-section (σ_{sc}) values between monomers and dimers (as depicted in Fig. 2c and d), with dimeric structures exhibiting lower σ_{sc} values compared to monomers structures. The desired condition for photothermal applications is characterized by high absorption cross-section (σ_{abs}) and low scattering cross-section (σ_{sc}).

Figures 2a and b indicate that the monomer with $AR_m = 6.1$ ($\lambda_p = 1040$ nm) and dimer with $AR_d = 10.1$ ($\lambda_p = 1041$ nm) exhibit their spectral peaks next to the typical used Nd: YAG laser (1064 nm), within the NIR biological window. In particular, the NR with AR=6.1 has a broad plasmonic peak (about 100 nm), which allows efficient excitation by 1064 nm illumination [19]. Moreover, Pedrosa et al. showed that photothermal conversion efficiency of NRs is not significantly affected by changing NR size (considering NR with length smaller than 100 nm) [7]. The NR monomer with $AR_m = 10.1$ shows $\lambda_p = 1410$ nm that is out of the biological window and far from the Nd: YAG laser line. Therefore, σ_{abs} and σ_{sc} of monomer are high at AR = 6.1 than that of AR 10.1 under the same excitation (1064 nm). On dealing with the gold nanorod colloidal heating, light polarization and the NP random orientation effects must be taken into account,

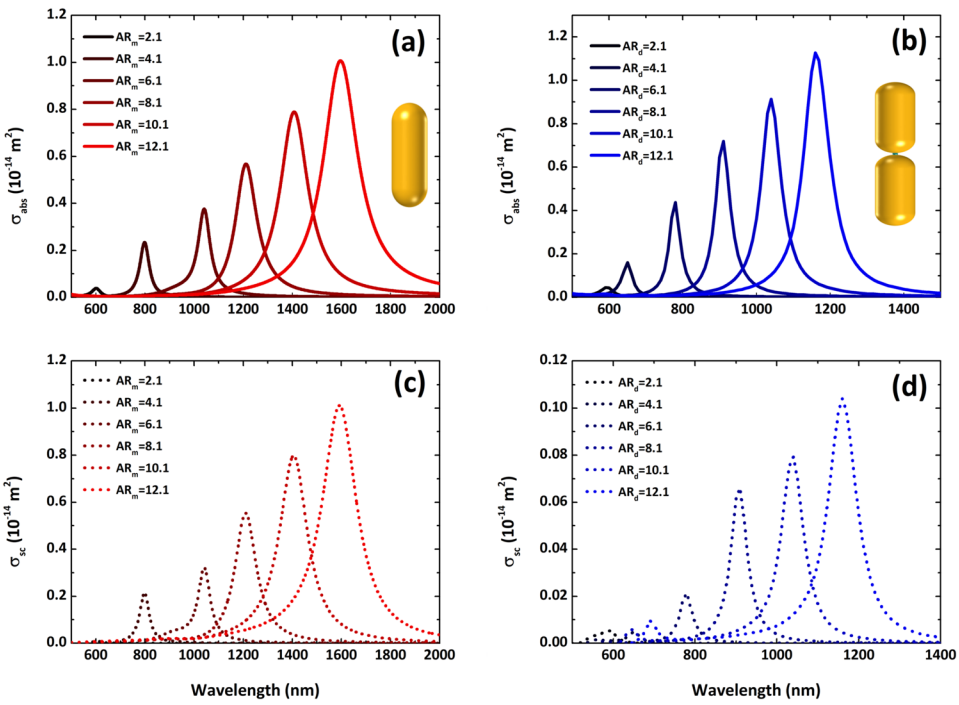

Fig. 2 Absorption (solid) and scattering (dotted) cross-sections spectrum of the Au nanostructures in water. **a** σ_{abs} of monomer and **b** dimer structures on tuning the aspect ratios. **c** σ_{sc} of monomers and **d** dimers with different aspect ratios

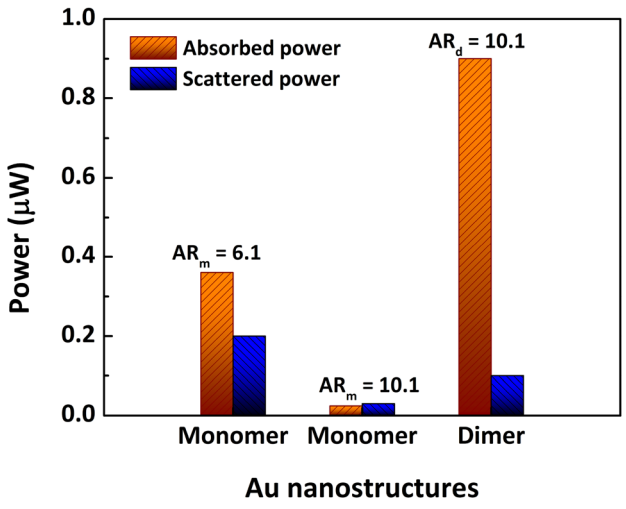

Fig. 3 Dissipated power (absorption and scattering powers) for gold monomers (AR_m) and dimeric (AR_d) structures in surrounding medium water

which may reduce the effective cross-section of the NR [11]. The absorbed and scattered power were analyzed by considering different ARs (6.1, 10.1) of monomer and dimeric structures (10.1). Figure 3 depicts that Au nanodimer possesses high absorption power ($P_{abs} = 8.4\ \mu$W) in comparison with monomer NR ($P_{abs} = 3.8\ \mu$W) under the irradiating laser intensity ($I = 1\times 10^9$ W/m^2) at 1064 nm wavelength. Different from Au monomers and dimeric structures, present absorption power is 8 times higher than the scattering that leads to high absorption efficiency ($\sigma_{abs}/\sigma_{ext}$) [35]. The high optical absorption power and absorption efficiency reinforce the use of Au NDs in biological thermal-related applications.

Localized Field Enhancement

Another important characteristic of LSPR structures is their ability to effectuate localized field enhancement nearby of nanoparticles. Such robust field enhancement could be exploited in applications such as imaging, SERS, biosensing, nonlinear optics, and controlled drug delivery. Here, we evaluate the field enhancement of an individual Au NR (6.1) and Au ND (10.1) under laser excitation at 1064 nm, as expounded in Fig. 4. One can see that the field enhancement of monomer nanorod is much lower than that of Au ND. The robust field in the dimer is due to the hot spot generated at the nanogap. One can see that the field enhancement of Au ND is 15× higher than single Au NR, explained by the presence of charge accumulation at the nanogap of gold ND.

As shown in Fig. 5, the localized field enhancement for Au ND can be better identified by exploring different spatial profiles of the electric field. The XY-plane, which is perpendicular to the incident field where a plane is a symmetry plane through the center of the dimer, is depicted in Fig. 5a. Figure 5c shows another cutting plane perpendicular to the polarization field and passing through the center of the nanogap. One can see that the hot spots are generated at the nanogap of the dimer, which is significantly higher than the other sides of the particle, as shown in Fig. 5b and d. This kind of hot spot cannot be produced in monomer nanostructures.

Thermal Analysis of Dimeric Structures

In order to quantify photothermal performance of a nanostructure, Lalisse and Co. [36] introduced a figure of merit, termed as a Joule number (J_0), that indicates the the ability of a NP to generate heat. The Joule number is defined as follows:

$$J_0 = \frac{\lambda_{ref} \times \sigma_{abs}}{2\pi V_{NP}} \tag{7}$$

where V_{NP} denotes particle volume, and λ_{ref} represents reference wavelength, i.e., photon wavelength with 1 eV energy. The use of J_0 is limited to analyses that consider non-cumulative short-pulse optical excitation [7].

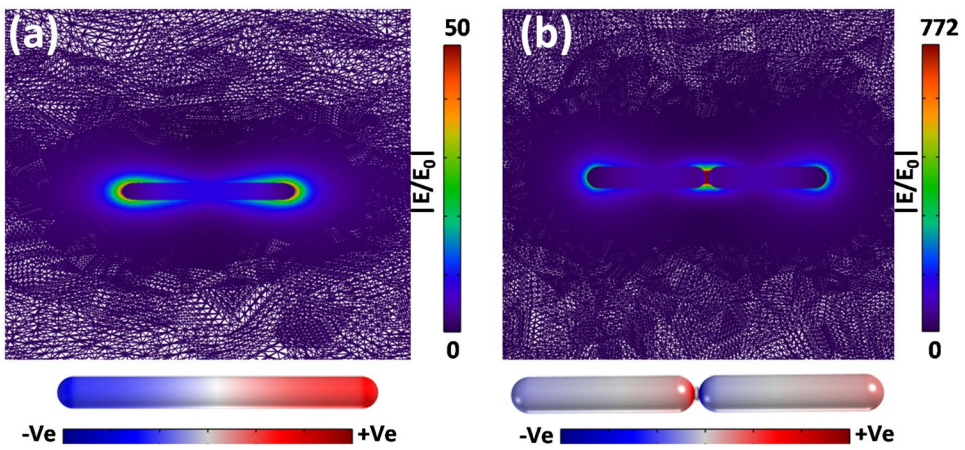

Fig. 4 Localized field enhancement and charge distribution of gold monomer NR (**a**) and dimeric rods (**b**)

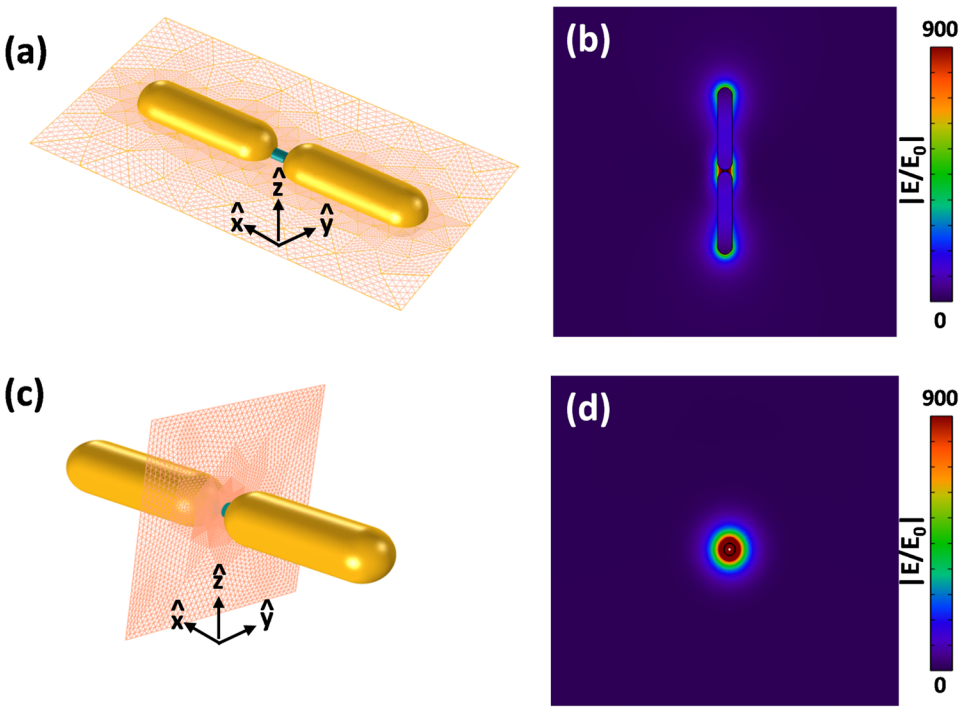

Fig. 5 The cutting planes of the gold dimeric metamolecule (**a**, **c**) were examined in relation to the orientation with respect to the field polarization under excitation by a 1064 nm wavelength laser and the respective distribution of localized E-field enhancement was analyzed (**b**, **d**)

In the case of the metamolecule with an aspect ratio (AR*D*) of 10.1, the joule number (J_0) of the NP was determined, as depicted in Fig. 6a. The efficiency of photothermal conversion for the Au ND is particularly prominent at the plasmonic resonance, specifically near the laser wavelength of 1064 nm. Furthermore, as the aspect ratio (length) of the ND increases, not only does the absorption cross-section (σ_{abs}) of the nanoparticle rise at resonance, but the volume of the nanostructure also increases, leading to a decrease in the joule number (J_0) values. Figure 6b illustrates the relationship between the metamolecule's J_0 and the particle AR, indicating that a ND with AR_D of 10.1 exhibits excellent performance in terms of infrared laser heating.

Figure 7 depicts temperature profiles of Au NR AR_m = 10.1 and Au ND AR_D = 10.1, obtained by Eq. (6) in water as a surrounding medium. Due to the hot spot effect in Au ND, a robust variation in temperature can be seen in dimeric structure than in monomer, as shown in Fig. 7a and b. The increase in temperature in Au ND is six times higher than that of monomer Au NR under the excitation at a specific laser line (1064 nm). In that case, the Au nanostructure temperature can rise more than 100 °C. The temperature rise is also observed in the surrounding medium but is limited to less than 100 nm from the particle surface, which could induce highly localized thermal damage. Figure 7c indicates the increased temperature at different distances from the particle surface.

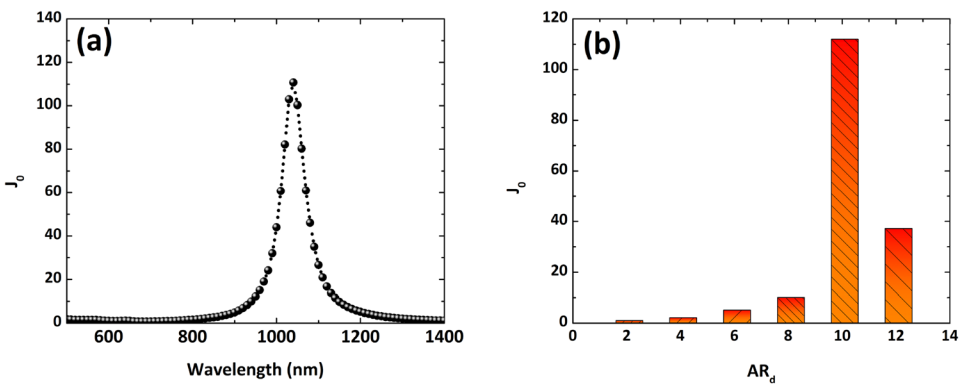

Fig. 6 **a** The joule number spectrum of Au ND with AR = 10.1. **b** Joule number values of dimeric structures with various aspect ratios, under 1064 nm laser excitation

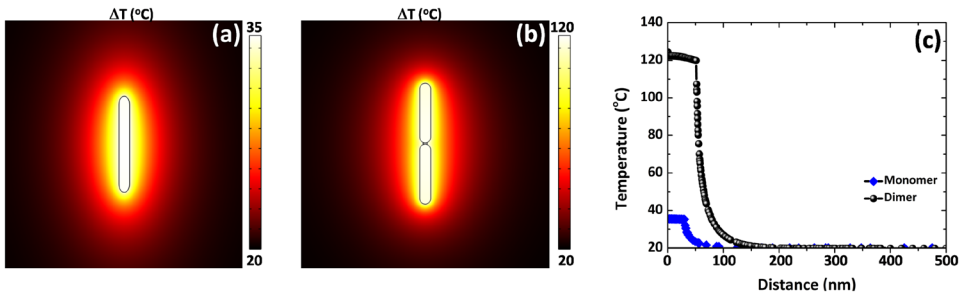

Fig. 7 Temperature distribution map around the monomer ($AR_m = 10.1$) (**a**) and dimeric ($AR_D = 10.1$) (**b**) nanostructure, under 1064 nm laser excitation. Steady-state temperature profile as a function of distance to center of nanostructures (**c**)

In the context of colloidal heating with pulsed polarized light, it is significant to consider the heating dynamics of both monomer and dimeric structures. The absorption cross-section serves as a useful parameter for estimating the transient temperature attained by the NPs, as depicted in Fig. 8. To validate our model for photothermal conversion, we refer to a case of heat transfer reported by Baffou et al. [34]. The temperature increase is more effective for the Au ND, which exhibits optimal absorption characteristics compared to the monomer Au NR. Under the excitation ($I = 1{\times}10^9$ W/m^2), higher transient temperatures are obtained for the Au ND. It takes approximately 20 ns for the ND to reach a steady-state temperature, whereas the monomer (smaller particle) requires a shorter excitation time to reach its maximum temperature. Therefore, nanosecond pulse lasers are suitable for efficiently exciting dimers, resulting in localized high temperatures.

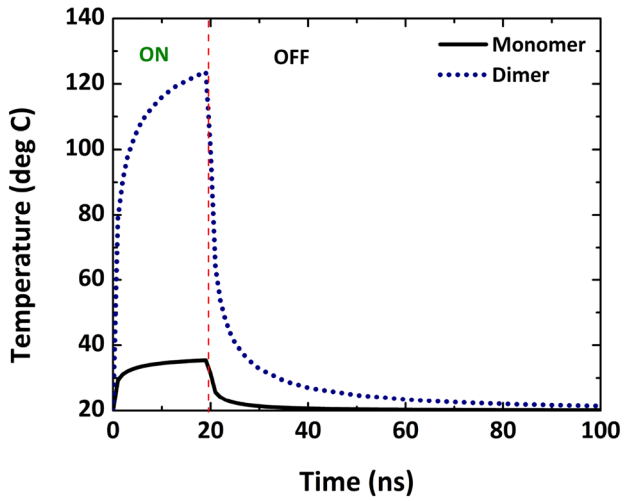

Fig. 8 The time-dependent temperature changes in Au ND and Au NR were evaluated under excitation by a 20 ns laser pulse with a power density of 1 mW/m^2 and a wavelength of 1064 nm

Conclusion

We have numerically investigated the photothermal conversion efficiency of gold dimeric structures by polarized light. The heating effects of such particles are effectively dependent on the dimeric structures' aspect ratio. By tuning the aspect ratios, the nanostructure LSPR peak is redshift, reaching the optical, biological window, and important laser lines as 1064 nm. The photothermal conversion ability was observed to be higher to the Au NDs structures than to monomer NR due to strong optical absorption. Nanodimers show robust hot spots localized at the nanostructure gap. Due to the high optical absorption power of Au ND, a robust increase in temperature is obtained up to 3.5× higher than that of monomer NRs under the same conditions. Moreover, *ns* laser excitation of Au ND can lead to a steady-state temperature increase, which is localized (<100nm) close to the dimer surface. Our computational framework simulation results establish a rational designing of Au NDs for high-performance thermal-assisted biological applications.

Author Contributions All authors contributed to the study conception and design. Material preparation, data collection, and analysis were performed by Sajid Farooq. The first draft of the manuscript was written by Sajid Farooq, Diego Rativa, and Renato E. de Araujo, and all authors commented on previous versions of the manuscript. All authors read and approved the final manuscript.

Funding The authors are grateful to Conselho Nacional de Desenvolvimento Científico e Tecnológico (CNPq), the National Institute of Science and Technology of Photonics (INCT de Fotônica), CNEN and the Coordenação de Aperfeiçoamento de Pessoal de Nível Superior 261 (CAPES) Finance Code 001.

Availability of Data and Materials The data generated during and/or analyzed during the current study is available from the corresponding author.

Declarations

Conflict of Interest The authors declare no competing interests.

References

1. Dreaden EC, Alkilany AM, Huang X, Murphy CJ, El-Sayed MA (2012) The golden age: gold nanoparticles for biomedicine. Chem Soc Rev 41:2740–2779
2. Farooq S, Neves WW, Pandoli O, Del Rosso T, de Lima LM, Dutra RF, de Araujo RE (2018) Engineering a plasmonic sensing platform for candida albicans antigen identification. J Nanophotonics 12(3):033003
3. Lu L, Zou S, Fang B (2021) The critical impacts of ligands on heterogeneous nanocatalysis: a review. ACS Catal 11:6020–6058
4. Cheng J, Liu N, Wang Y, Xuan X, Yang X, Zhou J (2020) Nitrogen-doped microporous carbon material decorated with metal nanoparticles derived from solid Zn/Co zeolitic imidazolate framework with high selectivity for CO2 separation. Fuel 265
5. Farooq S, Vital CVP, Gómez-Malagón LA, de Araujo RE, Rativa D (2020) Thermo-optical performance of iron-doped gold nanoshells-based nanofluid on direct absorption solar collectors. Sol Energy 208:1181–1188
6. Farooq S, Shafique S, Ahsan Z, Cardozo O, Wali F (2022) Tailoring the scattering response of optical nanocircuits using modular assembly. Nanomaterials 12(17):2962
7. Pedrosa TDL, Farooq S, de Araujo RE (2022) Selecting high-performance gold nanorods for photothermal conversion. Nanomaterials 12(23):4188
8. Baltar RMSM, Farooq S, de Araujo RE (2023) Selecting plasmonic nanoshells for colorimetric sensors. JOSA B 40(4):C40–C47
9. Mahmood HZ, Jilani A, Farooq S, Javed Y, Jamil Y, Iqbal J, Ullah S, Wageh S (2021) Plasmon-based label-free biosensor using gold nanosphere for dengue detection. Curr Comput-Aided Drug Des 11(11):1340
10. Farooq S, Wali F, Zezell DM, de Araujo RE, Rativam D (2022) Optimizing and quantifying gold nanospheres based on LSPR label-free biosensor for dengue diagnosis. Polymers 14(8):1592
11. Farooq S, Rativa D, de Araujo RE (2020) Orientation effects on plasmonic heating of near-infrared colloidal gold nanostructures. Plasmonics 15(5):1507–1515
12. Kelly KL, Coronado E, Zhao LL, Schatz GC (2003) The optical properties of metal nanoparticles: the influence of size, shape, and dielectric environment
13. Liu K, Xue X, Furlani EP (2016) Theoretical comparison of optical properties of near-infrared colloidal plasmonic nanoparticles. Sci Rep 6:34189
14. Farooq S, Rativa D, de Araujo RE (2019) Optimizing the sensing performance of SiO 2-Au nanoshells. Plasmonics 1–8
15. Păduraru DN, Ion D, Niculescu AG, Mușat F, Andronic O, Grumezescu AM, Bolocan A (2022) Recent developments in metallic nanomaterials for cancer therapy, diagnosing and imaging applications. Pharmaceutics 14(2):435
16. Yang W, Liang H, Ma S, Wang D, Huang J (2019) Gold nanoparticle based photothermal therapy: development and application for effective cancer treatment. Sustain Mater Technol 22
17. Shibu ES, Hamada M, Murase N, Biju V (2013) Nanomaterials formulations for photothermal and photodynamic therapy of cancer. J Photochem Photobiol, C 15:53–72
18. Schumacher L, Jose J, Janoschka D, Dreher P, Davis TJ, Ligges M, Li R, Mo M, Park S, Shen X et al (2019) Precision plasmonics with monomers and dimers of spherical gold nanoparticles: nonequilibrium dynamics at the time and space limits. J Phys Chem C 123(21):13181–13191
19. Farooq S, Rativa D, de Araujo RE (2021) High performance gold dimeric nanorods for plasmonic molecular sensing. IEEE Sens J 21(12):13184–13191
20. Farooq S, Rativa D, Said Z, de Araujo RE (2023) High performance blended nanofluid based on gold nanorods chain for harvesting solar radiation. Appl Therm Eng 218:119212
21. Zhu W, Esteban R, Borisov AG, Baumberg JJ, Nordlander P, Lezec HJ, Aizpurua J, Crozier KB (20160 Quantum mechanical effects in plasmonic structures with subnanometre gaps. Nat Commun 7(1):1–14
22. Hao Q, Huang H, Fan X, Hou X, Yin Y, Li W, Si L, Nan H, Wang H, Mei Y et al (2017) Facile design of ultra-thin anodic aluminum oxide membranes for the fabrication of plasmonic nanoarrays. Nanotechnology 28(10):105301
23. Zheng Y, Rosa L, Thai T, Ng SH, Gómez DE, Ohshima H, Bach U (2015) Asymmetric gold nanodimer arrays: electrostatic self-assembly and SERS activity. J Mater Chem A 3(1):240–249
24. Near R, Tabor C, Duan J, Pachter R, El-Sayed M (2012) Pronounced effects of anisotropy on plasmonic properties of nanorings fabricated by electron beam lithography. Nano Lett 12(4):2158–2164
25. Ikeda K, Takase M, Sawai Y, Nabika H, Murakoshi K, Uosaki K (2007) Hyper-Raman scattering enhanced by anisotropic dimer plasmons on artificial nanostructures. J Chem Phys 127(11)
26. Fontana J, Nita R, Charipar N, Naciri J, Park K, Dunkelberger A, Owrutsky J, Piqué A, Vaia R, Ratna B (2017) Widely tunable infrared plasmonic nanoantennas using directed assembly. Adv Opt Mater 5(21):1700335
27. Yoon K, Lee D, Kim JW, Kim J, Weitz DA (2012) Asymmetric functionalization of colloidal dimer particles with gold nanoparticles. Chem Commun 48(72):9056–9058
28. Chen G, Wang Y, Yang M, Xu J, Goh SJ, Pan M, Chen H (2010) Measuring ensemble-averaged surface-enhanced Raman scattering in the hotspots of colloidal nanoparticle dimers and trimers. J Am Chem Soc 132(11):3644–3645
29. Loo C, Lin A, Hirsch L, Lee MH, Barton J, Halas N, West J, Drezek R (2004) Nanoshell-enabled photonics-based imaging and therapy of cancer. Technol Cancer Res Treat 3(1):33–40
30. Mohamed MB, Ismail KZ, Link S, El-Sayed MA (1998) Thermal reshaping of gold nanorods in micelles. J Phys Chem B 102(47):9370–9374
31. Johnson PB, Christy RW (1972) Optical constants of the noble metals. Phys Rev B 6(12):4370
32. Farooq S, de Araujo RE (2018) Engineering a localized surface plasmon resonance platform for molecular biosensing. Open J Appl Sci 8(03):126
33. Yushanov S, Crompton JS, Koppenhoefer KC (2013) Mie scattering of electromagnetic waves. In Proceedings of the COMSOL Conference volume 116
34. Baffou G, Quidant R, de Abajo FJG (2010) Nanoscale control of optical heating in complex plasmonic systems. ACS Nano 4(2):709–716
35. Farooq S, Vital CVP, Gómez-Malagón LA, de Araujo RE, Rativa D (2020) Thermo-optical performance of iron-doped gold nanoshells-based nanofluid on direct absorption solar collectors. Sol Energy 208:1181–1188
36. Lalisse A, Tessier G, Plain J, Baffou G (2015) Quantifying the efficiency of plasmonic materials for near-field enhancement and photothermal conversion. J Phys Chem C 119(45):25518–25528